Reflection Removal Using Multiple Polarized Images with Different Exposure Times

Takuma AIZU
Faculty of Environmental Engineering
The University of Kitakyushu
Fukuoka, Japan
c1mca002@eng.kitakyu-u.ac.jp

Ryo MATSUOKA
Faculty of Environmental Engineering
The University of Kitakyushu
Fukuoka, Japan
r-matsuoka@kitakyu-u.ac.jp

***Abstract*—When we take a photograph through glass windows or doors, the foreground scene is reflected in the captured image. The reflected components overlap with the background scene and make object recognition and identification more difficult. This paper proposes a novel reflection removal method using multiple polarized images taken with different exposure times. To achieve a high accuracy reflection removal in high dynamic range scenes, in which photographed images have under-/over-exposed pixels, we introduce a minimization problem of weighted nonnegative matrix factorization (WNMF) with total variation regularization. To solve this minimization problem, we also introduce an alternating optimization scheme with the alternating direction method of multipliers (AO-ADMM). The advantages of the proposed method over some conventional methods are demonstrated in experiments of reflection removal using real-world images.**

***Index Terms*—Reflection removal, polarization, nonnegative matrix factorization, ADMM.**

I. Introduction

When we take a photograph through glass windows or doors, the foreground scene is reflected in the captured image. The reflected components overlap with the background scene and make object recognition and identification more difficult. For example, the recognition accuracy of objects is significantly decreased in in-vehicle/surveillance systems.

Let $\mathbf{t}$ and $\mathbf{r} \in \mathbb{R}^{3N}$ be vectorized color transmission and reflection components, respectively, where N is the number of pixels. Let $\mathbf{y} \in \mathbb{R}^{3N}$ be an observed image, we assume that an observed image is obtained by a convex combination of the transmission and reflection components as follows

$$\mathbf{y} = \alpha\mathbf{t} + \beta\mathbf{r}, \tag{1}$$

where α and β are positive multiplicative constants, i.e., blending coefficients of two components. According to this model, the problem of estimating two unknown transmission and reflection components from one observed image is NP-hard. To solve this problem, many reflection removal methods based on a priori information of a reflection component have been proposed [1]–[9]. Li and Brown [2] proposed a single image reflection removal method based on different relative smoothness properties between transmission and reflection components. Shibata et al. [5] proposed a reference-based reflection removal method by using a pair of RGB-D images based on the assumption that there is less reflection in the depth map even if it is taken through the glass.

Polarized imaging is known to be useful for removing reflections, and various polarized reflection removal methods have been introduced [1], [7], [9]. These methods assume that the reflection is partially polarized, and the relative intensity of the reflection can be adjusted by photographing through a linear polarizer. Farid and Adelson [1] separated the transmission and reflection components from multiple polarized images, which were taken with filters of different polarization angles, by using independent component analysis. However, this method requires a pair of polarization images taken with filters of polarization angles that maximize and minimize the intensity of the reflected component, respectively. In addition, there is a problem that the separated components have negative values. Lei et al. [9] introduced a deep learning-based reflection removal method. However, learning-based approaches require a large amount of training data set obtained in a variety of scenes. Moreover, under-/over-exposed pixels occur in high dynamic range scenes such as backlight and low-light conditions [10]–[14], and make it even more difficult to separate reflections. These problems due to under/over-exposed pixels, which depend on photographing scenes, are common problems to be solved in both non-learning and learning based reflection removal methods.

In this paper, we propose a novel reflection removal method by using multiple polarized images with different exposure times. To achieve reflection removal in high dynamic range scenes, where photographed images have under-/over-exposed pixels, we introduce a minimization problem of weighted nonnegative matrix factorization (WNMF) with total variation regularization. To solve the proposed problem, we also introduce an alternating optimization scheme with the alternating direction method of multipliers (AO-ADMM). Experimental results demonstrate the effectiveness of the proposed method compared with some conventional methods.

The paper is organized as follows. In Section II, we present several mathematical preliminaries to introduce the proposed method. Section III introduces a novel reflection removal method for multiple polarized images with different exposure times. In Section IV, several examples are shown to verify the validity of our method. Finally, we conclude this paper in

Section V.

II. Preliminaries

A. Nonnegative matrix factorization

Nonnegative matrix factorization (NMF) [15] is a matrix decomposition method that decomposes an observed data matrix $\mathbf{V}$ composed of nonnegative values into two nonnegative matrices $\mathbf{W}$ and $\mathbf{H}$ that satisfy $\mathbf{V} \simeq \mathbf{W}\mathbf{H}^\top$. The transpose of a vector or a matrix is defined by $(\cdot)^\top$. The solution of this decomposition problem is obtained by minimizing an objective function $\mathcal{D}(\mathbf{W}, \mathbf{H})$, which is the degree of the divergence between $\mathbf{V}$ and $\mathbf{W}\mathbf{H}^\top$. The function $\mathcal{D}(\mathbf{W}, \mathbf{H})$ is generally defined by

$$\mathcal{D}(\mathbf{W}, \mathbf{H}) = \left\| \mathbf{V} - \mathbf{W}\mathbf{H}^\top \right\|_F^2, \tag{2}$$

where $\|\cdot\|_F$ is the Frobenius norm. To solve the minimization problem (2), multiplicative update algorithms, gradient descent algorithms, and alternating least squares (ALS) algorithms are often used.

B. Alternating Direction Method of Multipliers

Alternating direction method of multipliers (ADMM) [16] is a proximal splitting algorithm that can treat convex optimization problems of the form

$$\min_{\mathbf{x}\in\mathbb{R}^{N_1},\, \mathbf{z}\in\mathbb{R}^{N_2}} F(\mathbf{x}) + G(\mathbf{z}) \;\text{ s.t. }\; \mathbf{z} = \mathbf{L}\mathbf{x}, \tag{3}$$

where F and G are usually assumed to be a quadratic and proximable function, respectively, and $\mathbf{L} \in \mathbb{R}^{N_2\times N_1}$ is a matrix with full-column rank. For any $\mathbf{x}^{(0)} \in \mathbb{R}^{N_1}, \mathbf{z}^{(0)} \in \mathbb{R}^{N_2}, \mathbf{b}^{(0)} \in \mathbb{R}^{N_2}$ and $\gamma > 0$, the ADMM algorithm is given by

$$\begin{cases} \mathbf{x}^{(t+1)} = \arg\min_{\mathbf{x}} \left\{ F(\mathbf{x}) + \dfrac{\gamma}{2}\|\mathbf{z}^{(t)} - \mathbf{L}\mathbf{x} - \mathbf{b}^{(t)}\|_2^2 \right\}, \\ \mathbf{z}^{(t+1)} = \arg\min_{\mathbf{z}} \left\{ G(\mathbf{z}) + \dfrac{\gamma}{2}\|\mathbf{z} - \mathbf{L}\mathbf{x}^{(t+1)} - \mathbf{b}^{(t)}\|_2^2 \right\}, \\ \mathbf{b}^{(t+1)} = \mathbf{b}^{(t)} + \mathbf{L}\mathbf{x}^{(t+1)} - \mathbf{z}^{(t+1)}, \end{cases} \tag{4}$$

where the superscript (t) denotes the iteration number. The sequence generated by (4) quickly converges to an optimal solution of (3).

C. Total Variation

By letting $\mathbf{D}_v$ and $\mathbf{D}_h \in \mathbb{R}^{N\times N}$ be the vertical and horizontal first-order differential operators, respectively, with Neumann boundaries, the differential operator is expressed by $\mathbf{D} := [\mathbf{D}_v^\top \; \mathbf{D}_h^\top]^\top \; \left(\in \mathbb{R}^{2N\times N}\right)$ for a vectorized gray image with N pixels, and thus the total variation (TV) is defined as [17], [18]

$$\|\mathbf{x}\|_{\mathrm{TV}} := \|\mathbf{D}\mathbf{x}\|_{1,2} = \sum_{i=1}^{N} \sqrt{(\mathbf{D}_v\mathbf{x})_i^2 + (\mathbf{D}_h\mathbf{x})_i^2}, \tag{5}$$

where $(\mathbf{D}_v\mathbf{x})_i$ and $(\mathbf{D}_h\mathbf{x})_i$ are the i-th element of $\mathbf{D}_v\mathbf{x}$ and $\mathbf{D}_h\mathbf{x}$, respectively.

The minimization problem with TV regularization is defined as

$$\mathbf{x}^\star = \arg\min_{\mathbf{x}} \|\mathbf{x}\|_{\mathrm{TV}} + \frac{\lambda}{2}\|\mathbf{x} - \mathbf{x}_{\mathrm{in}}\|_2^2, \tag{6}$$

where $\mathbf{x}_{\mathrm{in}}$ is a vectorized input image and $\lambda > 0$ is a balancing weight of two terms.

III. Proposed Method

A. Reflection removal model for polarization images

When an image is taken with a linear polarizer filter of polarization angle θ, the observation model defined in (1) can be redefined as follows[1]

$$\mathbf{y}_\theta = \alpha_\theta \mathbf{t} + \beta_\theta \mathbf{r}. \tag{7}$$

Furthermore, given the polarized images of the polarization angles $\theta_1, \ldots, \theta_M$, we obtain the following M equations

$$\begin{aligned} \mathbf{y}_{\theta_1} &= \alpha_{\theta_1}\mathbf{t} + \beta_{\theta_1}\mathbf{r}, \\ &\vdots \\ \mathbf{y}_{\theta_M} &= \alpha_{\theta_M}\mathbf{t} + \beta_{\theta_M}\mathbf{r}. \end{aligned} \tag{8}$$

Then, we obtain the following equation that expresses these equations in matrix form

$$\mathbf{Y} = \mathbf{W}\mathbf{H}^\top, \tag{9}$$

where $\mathbf{Y} := [\mathbf{y}_{\theta_1} \ldots \mathbf{y}_{\theta_M}] \; \left(\in \mathbb{R}^{3N\times M}\right)$ is a matrix of M polarization images, $\mathbf{W} := [\mathbf{t}\; \mathbf{r}] \; \left(\in \mathbb{R}^{3N\times 2}\right)$ is a matrix that arranges the transmission and reflection components, and

$$\mathbf{H} := \begin{bmatrix} \alpha_{\theta_1} & \cdots & \alpha_{\theta_M} \\ \beta_{\theta_1} & \cdots & \beta_{\theta_M} \end{bmatrix}^\top \left(\in \mathbb{R}^{M\times 2}\right)$$

is a matrix of positive multiplicative constants, and each column consists of the coefficients of each component.

In the case of a high dynamic range scene, images often have under-/over-exposed pixels due to under-/over-exposure. Since the observation model (9) is not valid for such pixels, we consider the use of multiple exposure images. The observation model for the k-th exposure image $\mathbf{Y}_k := [\mathbf{y}_{\theta_1,k} \ldots \mathbf{y}_{\theta_M,k}] \; \left(\in \mathbb{R}^{3N\times M}\right)$[2] is defined by

$$\mathbf{Y}_k = \mathbf{W}\mathbf{H}_k^\top := \mathbf{W}\mathbf{H}^\top e_k, \tag{10}$$

where e_k is the k-th exposure time. We assume that the scale variation of pixel values of each exposure image caused by each exposure time does not affect the latent components, but the multiplication coefficients. Thus, we introduce $\mathbf{H}_k := \mathbf{H}e_k$. Each exposure image is generated by blending the same scale transmission and reflection components $\mathbf{W}$ using their multiplication matrix $\mathbf{H}_k$.

B. Minimization problem

Our aim is to estimate the transmission and reflection layer from multiple polarized images with different exposure times. We propose a weighted nonnegative matrix factorization problem to reduce model errors caused by under-/over-exposed pixels, and then introduce the TV regularization to enhance the

[1] The dynamic range of images is normalized in $[0, 1]$.

[2] Note that the multiple exposure images are linearized to the irradiance of scenes.

smoothness of the latent components. The proposed minimization problem is defined by

$$\min_{\mathbf{W},\mathbf{H}_1,\ldots,\mathbf{H}_K} \sum_{k=1}^{K} \left\|\mathbf{M}_k \circ \left(\mathbf{Y}_k - \mathbf{W}\mathbf{H}_k^\top\right)\right\|_F^2 + \sum_{l=1}^{2} \lambda_l \|\mathbf{w}_l\|_{\mathrm{TV}}$$
$$\text{s.t. } \mathbf{W} \in \mathbb{R}_+^{3N\times 2},\ \ \mathbf{H}_k \in \mathbb{R}_+^{M\times 2}\ \ \forall_k,\ \ \|\mathbf{w}_l\|_\infty = 1\ \ \forall_l, \tag{11}$$

where $\mathbb{R}_+$ denotes the set of all nonnegative real numbers, $\lambda_l\,(l = 1, 2)$ is a balancing weight, which controls the smoothness of each component, and the operator $\circ$ denotes element-wise multiplication. The matrix $\mathbf{M}_k$ $\left(\in \mathbb{R}^{3N\times M}\right)$ is a masking matrix defined by

$$\mathbf{M}_k := [\mathrm{diag}(\mathcal{M}(\mathbf{y}_{\theta_1,k}))\ \ldots\ \mathrm{diag}(\mathcal{M}(\mathbf{y}_{\theta_M,k}))],$$

where $\mathcal{M}(\cdot)$ is a masking function to avoid under-/over-exposed pixels and defined by

$$\mathcal{M}(x) := \begin{cases} 1, & \text{if } \ \underline{\xi} \le x \le \overline{\xi} \\ \epsilon_s, & \text{otherwise} \end{cases}, \tag{12}$$

where $\underline{\xi}$ and $\overline{\xi}$ are lower-/upper-bound of pixel values, and ϵ_s is a small value.

The first term of (11) is the sum of a fidelity term for multiple exposure polarized images derived from (10). The second term of (11) is the TV regularization defined in (5). The first and second constraints are nonnegative constraints for the matrices $\mathbf{W}$ and $\mathbf{H}_k$, respectively. The third constraint[3] is a constraint to normalize the maximum value of each latent component, i.e., transmission and reflection components, respectively, to 1.

C. Optimization

The proposed minimization problem (11) is nonconvex due to the product of two objective variables $\mathbf{W}$ and $\mathbf{H}_k$. To find that solution, we propose an alternating optimization approach based on ADMM. The proposed problem (11) can be separated into two subproblems w.r.t. each of the objective variables $\mathbf{H}_k$ and $\mathbf{W}$ with other variables fixed as follows

$$\min_{\mathbf{H}_1,\ldots,\mathbf{H}_K} \sum_{k=1}^{K} \left\|\mathbf{M}_k \circ \left(\mathbf{Y}_k - \mathbf{W}\mathbf{H}_k^\top\right)\right\|_F^2 \quad \text{s.t. } \mathbf{H}_k \in \mathbb{R}_+^{M\times 2}\ \ \forall_k, \tag{13}$$

$$\min_{\mathbf{W}} \sum_{k=1}^{K} \left\|\mathbf{M}_k \circ \left(\mathbf{Y}_k - \mathbf{W}\mathbf{H}_k^\top\right)\right\|_F^2 + \sum_{l=1}^{2} \lambda_l \|\mathbf{w}_l\|_{\mathrm{TV}} \quad \text{s.t. } \mathbf{W} \in \mathbb{R}_+^{3N\times 2},\ \ \|\mathbf{w}_l\|_\infty = 1\ \ \forall_l. \tag{14}$$

Since each subproblem is convex, we can alternatively find the optimal solution of each problem by using ADMM, called AO-ADMM [20]–[22]. The whole algorithm is shown in Algorithm 1.

[3]Nonnegative matrix factorization has the problem of scale ambiguity [15], [19]. That is, the scales of the basis matrix W and the coefficient matrix H are not uniquely determined. To tackle this problem, we constraint the maximum value of $\mathbf{w}_1$ and $\mathbf{w}_2$, respectively.

Algorithm 1 Proposed AO-ADMM algorithm

1: **Input** : $\mathbf{W}^{(0)}, \mathbf{H}_k^{(0)}, \mathbf{Y}_k, \mathbf{M}_k\ (k = 1, \ldots, K),\ \lambda_1, \lambda_2, \tau = 0$;
2: **Output** : $\mathbf{W}^{(\tau)}, \mathbf{H}_k^{(\tau)} (k = 1, \ldots, K)$;
3: **while** A stopping criterion is not satisfied **do**
4: Update $\mathbf{H}_k\ (k = 1, \ldots, K)$ by solving (13) using ADMM algorithm with $\mathbf{W}^{(\tau)}$;
5: Update $\mathbf{W}$ by solving (14) using the ADMM algorithm with $\mathbf{H}_k^{(\tau+1)}\ (k = 1, \ldots, K)$;
6: $\tau = \tau + 1$;
7: **end while**

In the standard NMF algorithm, the objective variables $\mathbf{W}$ and $\mathbf{H}$ are initialized with random nonnegative values [15]. However, initialization with random nonnegative values has little chance to obtain a reasonable solution, and the convergence speed of the algorithm may also be slow. To address this issue, we calculate an image with the minimum value of input multiple polarized images in each pixel, in which under-exposed pixels are avoided, and set it as the initial value of the transmission component $\mathbf{w}_1$. The other variables are initialized with random nonnegative values.

IV. Experiments

To demonstrate the effectiveness of the proposed method, we applied it to the real-world image data sets captured by using FLIR BFS-U3-51S5-C[4], where we used a tripod to avoid camera shake. Note that multiple polarized images were taken with different exposure times ($K = 3$), in which, short-, middle-, and long-exposure polarized images were obtained in each scene (see Fig. 1). We compared our method with Farid and Adelson's method [1], which is the polarized image reflection removal method, and Li and Brown's method [2], which is the single image reflection removal method. Both methods do not assume the use of multiple exposure images, i.e., under-/over-exposed images. Thus, we used a polarized high dynamic range (HDR) image obtained by blending input multiple exposure (polarized) images using a standard exposure blending method [10][5] as input images for the conventional methods. Since Farid and Adelson's method requires two polarized images with a different polarization angle, we choose the results of a pair of polarized HDR images in $\{\theta = 0°, 45°, 90°, 135°\}$ which having the highest quantitative evaluation values. For input images of Li and Brown's method, we used the averaged image of four polarized HDR images.

For quantitative evaluation, we also obtained "Ground truth" HDR transmission components by blending multiple polarized images with different exposure times, which were taken by physically removing the portable glass as in [6]. Note that the camera parameters were fixed, i.e., these images were captured with the same exposure times of the polarized reflection images. For the quality metrics, we used PSNR, SSIM [23], and SI [3][6]. Since the pixel scale of the reflection removal results

[4]This camera can capture four polarization angle RGB images in one shot.
[5]Note that we used Gaussian type hat-function for calculating weight maps.
[6]The radius of Gaussian filter used in SSIM and SI was set to 3 in order to make the score vary depending on the presence or absence of reflections.

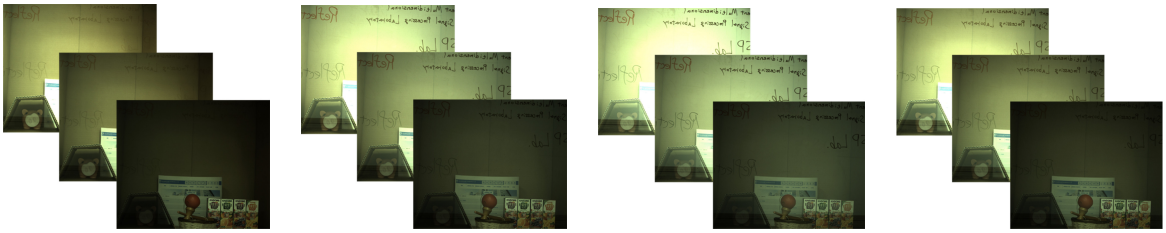

$\theta = 0°$ $\theta = 45°$ $\theta = 90°$ $\theta = 135°$

Fig. 1. Example of input polarized images in Scene 1: (front to back) short-, middle-, and long-exposure images.

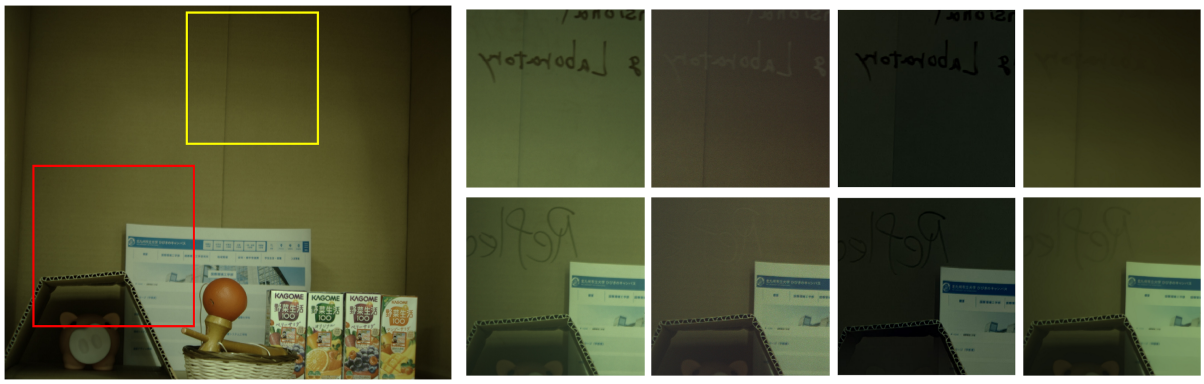

(a) (b) (c) (d) (e)

Fig. 2. Results of Scene 1: (a) Ground truth, (b) input scene with reflection, (c) Farid and Adelson [1], (d) Li and Brown [2], and (e) ours.

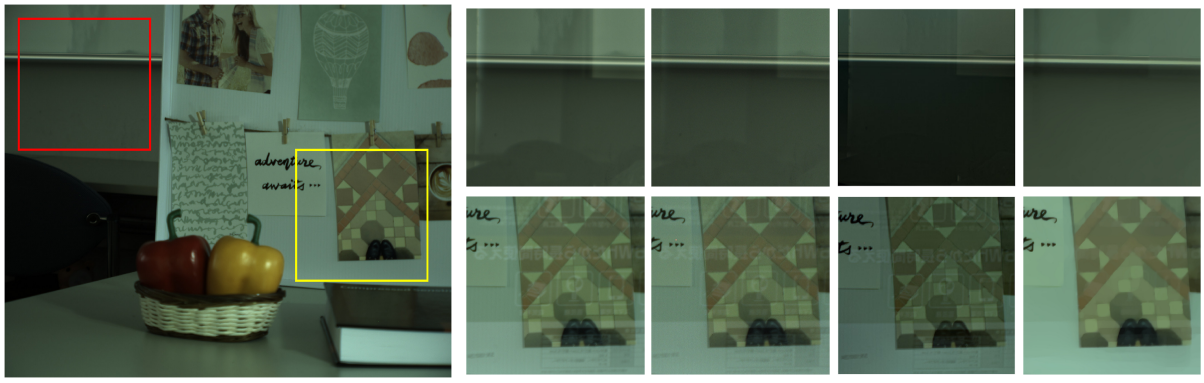

(a) (b) (c) (d) (e)

Fig. 3. Results of Scene 2: (a) Ground truth, (b) input scene with reflection, (c) Farid and Adelson [1], (d) Li and Brown [2], and (e) ours.

estimated by our method and the conventional methods are ambiguous, we adjusted its scale so that to the same pixel scale of the Ground truth images for fair quantitative evaluation. All experiments were performed using MATLAB on an Ubuntu Linux desktop computer with an AMD EPYC 7402P 2.8GHz CPU and 128 GB RAM. To accelerate the computation time of the proposed method, we used an NVIDIA GeForce RTX 3090 GPU. For the parameters of our method, we set $\underline{\xi} = 2/255$, $\overline{\xi} = 253/255$, and $\epsilon_s = 10^{-1}$ in all experiments. Then, we found the visually best results by adjusting λ_1, where we set $\lambda_2 = 5.0 \cdot 10^{-2}\lambda_1$. For the parameter setting of Li and Brown's method, we also found the visually best results for fair comparison.

Figures 2 and 3 show the Ground truth images and some closeup images in Scenes 1 and 2, respectively. One observes from both figures that our method outperforms the conventional methods. As can be seen from Fig. 2 (b), which is the average of the polarized HDR images obtained by blending multiple polarized images, the reflection of the characters can be seen. In the results of Farid and Adelson's method, we can see that the text of the reflection component remained and reversed its color from black to white, especially in the first row of Fig. 2 (c). This artifact is also slightly visible in the second row of Fig. 2 (c). In Fig. 2 (d), Li and Brown's method cannot remove the reflection component having sharper edges. This is because this method assumes that the reflection component has small edges due to out-of-focus, and does not work well in such scenes where the reflected

TABLE I
QUANTITATIVE COMPARISON RESULTS.

	PSNR				SSIM				SI			
Method \ Scene	1	2	3	4	1	2	3	4	1	2	3	4
Farid and Adelson [1]	21.40	27.47	25.03	22.25	0.8236	0.9051	0.8804	0.7075	0.9270	0.9549	0.9471	0.8365
Li and Brown [2]	19.87	24.00	21.36	21.10	0.8024	0.8779	0.8359	0.8430	0.9476	0.9555	0.9742	0.9245
Ours	**27.28**	**28.58**	**32.38**	**28.32**	**0.9223**	**0.9308**	**0.9741**	**0.9271**	**0.9766**	**0.9704**	**0.9907**	**0.9609**

component is also in focus.

In contrast, our method shown in Fig. 2 (e) can remove the reflection component with higher accuracy. We see from Figs. 3 (c) and (d) that both of the conventional methods cannot remove the reflection component, while our method shown in Fig. 3 (e) can remove the reflection component significantly better than the conventional method.

Table I shows the PSNR, SSIM, and SI comparison results. One can observe from Table I that our method has the highest value in all quantitative evaluations compared with the other methods in all the scenes.

V. CONCLUSIONS

This paper proposed a novel reflection removal method for multiple polarized images with different exposure times. We introduced a weighted nonnegative matrix factorization (WNMF) with total variation (TV) regularization, and solved it by using an alternating optimization scheme with the alternating direction method of multipliers (AO-ADMM). WNMF reduces model errors caused by under-/over-exposed pixels, and then the TV regularization promotes the local smoothness of the transmission and reflection components, resulting in highly accurate reflection removal. Experiments confirmed that the proposed method outperforms some existing methods.

In future works, we will attempt to improve the computational efficiency of the proposed alternating optimization algorithm by employing stochastic gradient descent algorithms.

ACKNOWLEDGMENT

This work was partially supported by JSPS KAKENHI Grant Number 20H00612 and 21K17767.

REFERENCES

[1] H. Farid and E. Adelson, "Separating reflections and lighting using independent components analysis," in *Proceedings. 1999 IEEE Computer Society Conference on Computer Vision and Pattern Recognition (Cat. No PR00149)*, vol. 1, 1999, pp. 262–267 Vol. 1.

[2] Y. Li and M. S. Brown, "Single image layer separation using relative smoothness," in *2014 IEEE Conference on Computer Vision and Pattern Recognition*, 2014, pp. 2752–2759.

[3] R. Wan, B. Shi, L.-Y. Duan, A.-H. Tan, and A. C. Kot, "Benchmarking single-image reflection removal algorithms," in *2017 IEEE International Conference on Computer Vision (ICCV)*, 2017, pp. 3942–3950.

[4] R. Matsuoka, "Reflection removal based on gradient constraints," in *2017 IEEE 6th Global Conference on Consumer Electronics (GCCE)*, 2017, pp. 1–2.

[5] T. Shibata, Y. Akai, and R. Matsuoka, "Reflection removal using rgb-d images," in *2018 25th IEEE International Conference on Image Processing (ICIP)*, 2018, pp. 1862–1866.

[6] X. Zhang, R. Ng, and Q. Chen, "Single image reflection separation with perceptual losses," in *Proceedings of the IEEE conference on computer vision and pattern recognition*, 2018, pp. 4786–4794.

[7] Y. Lyu, Z. Cui, S. Li, M. Pollefeys, and B. Shi, "Reflection separation using a pair of unpolarized and polarized images," in *Advances in Neural Information Processing Systems*, vol. 32. Curran Associates, Inc., 2019.

[8] A. Punnappurath and M. S. Brown, "Reflection removal using a dual-pixel sensor," in *2019 IEEE/CVF Conference on Computer Vision and Pattern Recognition (CVPR)*, 2019, pp. 1556–1565.

[9] C. Lei, X. Huang, M. Zhang, Q. Yan, W. Sun, and Q. Chen, "Polarized reflection removal with perfect alignment in the wild," in *2020 IEEE/CVF Conference on Computer Vision and Pattern Recognition, CVPR 2020, Seattle, WA, USA, June 13-19, 2020*. Computer Vision Foundation / IEEE, 2020, pp. 1747–1755.

[10] P. E. Debevec and J. Malik, "Recovering high dynamic range radiance maps from photographs," in *Proceedings of the 24th Annual Conference on Computer Graphics and Interactive Techniques*, ser. SIGGRAPH '97. USA: ACM Press/Addison-Wesley Publishing Co., 1997, p. 369–378.

[11] T. Jinno and M. Okuda, "Multiple exposure fusion for high dynamic range image acquisition," *IEEE Transactions on Image Processing*, vol. 21, no. 1, pp. 358–365, 2012.

[12] R. Matsuoka, S. Ono, and M. Okuda, "High dynamic range image generation based on convolutional weight optimization robust to mixed noise removal," in *2018 Asia-Pacific Signal and Information Processing Association Annual Summit and Conference (APSIPA ASC)*, 2018, pp. 1066–1070.

[13] R. Matsuoka, K. Shirai, and M. Okuda, "Reference-based local color distribution transformation method and its application to image integration," *Sig. Process.: Image Comm.*, vol. 76, pp. 231 – 242, 2019.

[14] R. Matsuoka, S. Ono, and M. Okuda, "Transformed-domain robust multiple-exposure blending with huber loss," *IEEE Access*, vol. 7, pp. 162 282–162 296, 2019.

[15] M. W. Berry, M. Browne, A. N. Langville, V. P. Pauca, and R. J. Plemmons, "Algorithms and applications for approximate nonnegative matrix factorization," *Computational Statistics & Data Analysis*, vol. 52, no. 1, pp. 155–173, 2007.

[16] D. Gabay and B. Mercier, "A dual algorithm for the solution of nonlinear variational problems via finite element approximation," *Comput. & Math. Appl.*, vol. 2, no. 1, pp. 17 – 40, 1976.

[17] X. Bresson and T. F. Chan, "Fast dual minimization of the vectorial total variation norm and applications to color image processing," *Inverse Probl. Imag.*, vol. 2, no. 4, pp. 455–484, 2008.

[18] P. L. Combettes and J.-C. Pesquet, "A proximal decomposition method for solving convex variational inverse problems," *Inverse Probl.*, vol. 24, no. 6, p. 065014, 2008.

[19] R. Oya., R. Matsuoka., and T. Okabe., "NMF vs. ICA for light source separation under AC illumination," in *Proceedings of the 15th International Joint Conference on Computer Vision, Imaging and Computer Graphics Theory and Applications - Volume 4: VISAPP,*, INSTICC. SciTePress, 2020, pp. 460–465.

[20] K. Huang, N. D. Sidiropoulos, and A. P. Liavas, "A flexible and efficient algorithmic framework for constrained matrix and tensor factorization," *IEEE Transactions on Signal Processing*, vol. 64, no. 19, pp. 5052–5065, 2016.

[21] S. Ono and T. Kasai, "Efficient constrained tensor factorization by alternating optimization with primal-dual splitting," in *2018 IEEE International Conference on Acoustics, Speech and Signal Processing (ICASSP)*, 2018, pp. 3379–3383.

[22] M. Roald, C. Schenker, J. E. Cohen, and E. Acar, "Parafac2 ao-admm: Constraints in all modes," in *2021 29th European Signal Processing Conference (EUSIPCO)*, 2021, pp. 1040–1044.

[23] Z. Wang, A. Bovik, H. Sheikh, and E. Simoncelli, "Image quality assessment: from error visibility to structural similarity," *IEEE Trans. Image Process.*, vol. 13, no. 4, pp. 600–612, 2004.